

Superconducting fluctuations and charge-4e plaquette state at strong coupling

Qiong Qin,^{1,2} Jian-Jun Dong,³ Yutao Sheng,^{1,2} Dongchen Huang,^{1,2} and Yi-feng Yang^{1,2,4,*}

¹*Beijing National Laboratory for Condensed Matter Physics and Institute of Physics,
Chinese Academy of Sciences, Beijing 100190, China*

²*University of Chinese Academy of Sciences, Beijing 100049, China*

³*Department of Physics and Chongqing Key Laboratory for Strongly Coupled Physics,
Chongqing University, Chongqing 401331, China*

⁴*Songshan Lake Materials Laboratory, Dongguan, Guangdong 523808, China*

(Dated: August 15, 2023)

We apply the static auxiliary field Monte Carlo approach to study phase correlations of the pairing fields in a model with spin-singlet pairing interaction. We find that the short- and long-distance phase correlations are well captured by the phase mutual information, which allows us to construct a theoretical phase diagram containing the uniform d -wave superconducting region, the phase fluctuating region, the local pairing region, and the disordered region. We show that the gradual development of phase coherence has a number of consequences on spectroscopic measurements, such as the development of the Fermi arc and the anisotropy in the angle-resolved spectra, scattering rate, entropy, specific heat, and quasiparticle dispersion, in good agreement with experimental observations. For strong coupling, our Monte Carlo simulation reveals an unexpected charge-4e plaquette state with d -wave bonds, which competes with the uniform d -wave superconductivity and exhibits a U-shaped density of states.

I. INTRODUCTION

Superconducting fluctuations have been proposed to play an important role in underdoped cuprates¹⁻¹⁴. Their presence may be responsible for the back bending bands above the superconducting transition temperature T_c ¹⁵, continuous variation of the spectral gap across the transition¹⁶, and probably the large Nernst effect and diamagnetic signals¹⁷. They have also been used to explain the mysterious pseudogap state¹⁸⁻³⁶, but negated by some experiments showing that superconducting fluctuations only exist in a much narrower region than the pseudogap³⁷. Their interplay with competing orders may be the cause of particle-hole asymmetry³⁸, time-reversal symmetry breaking^{38,39}, or rotational symmetry breaking⁴⁰ observed in some materials.

In overdoped cuprates, mean-field analyses have been widely used to describe superconductivity, since it correctly predicted the d -wave pairing and the decrease in T_c with hole density¹, while superconducting fluctuations have scarcely been considered seriously⁴¹, although experiments have reported a linear relation between the superfluid density and T_c and thus highlighted the crucial role of superconducting phase stiffness^{42,43}. Very recently, the angle-resolved photoemission spectroscopy (ARPES) observation of a d -wave gap and particle-hole symmetric dispersion above T_c in overdoped $\text{Bi}_2\text{Sr}_2\text{CaCu}_2\text{O}_{8+\delta}$ ⁴⁴⁻⁴⁶ has stimulated intensive debates concerning the existence of phase fluctuations in overdoped cuprates and whether the observed anomalous properties are due to superconducting fluctuations or involve other mechanisms such as anisotropic impurity scattering⁴⁷.

In this work, we explore the potential consequences of superconducting fluctuations on the spectroscopic observations in overdoped cuprates. Different from pre-

vious studies^{14,47-50}, we employ a static auxiliary field Monte Carlo approach⁵¹⁻⁵⁶ and use phase mutual information to analyze short- and long-range phase correlations of the superconducting pairing fields. The mutual information⁵⁷⁻⁶³ measures the nonlinear association of the probabilistic distribution⁶⁴⁻⁶⁶ and has been successfully applied to various physical systems⁶⁷⁻⁷². It provides an excellent indicator of superconducting phase correlation and allows us to construct a superconducting phase diagram with the temperature and pairing interaction. We identify three temperature scales over a wide intermediate range of the pairing interaction, and we determine four distinct phases: the superconducting, (macroscopic) phase fluctuating, local pairing, and disordered regions. Calculations of the angle-resolved spectra, scattering rate, entropy, specific heat, quasiparticle dispersion, and Fermi arc show interesting anisotropic features, beyond the mean-field theory but agreeing well with experiments. For sufficiently strong pairing interaction, we find a plaquette state of charge-4e pairing with a U-shaped density of states that competes with the uniform d -wave superconductivity⁷³. Our work provides a systematic understanding of the effects of superconducting fluctuations on the spectroscopic properties in overdoped cuprates.

II. MODEL AND METHOD

We start with the following Hamiltonian,

$$H = - \sum_{i\ell\sigma} t_{i\ell} c_{i\sigma}^\dagger c_{\ell\sigma} - \mu \sum_{i\sigma} c_{i\sigma}^\dagger c_{i\sigma} - V \sum_{\langle ij \rangle} (\psi_{ij}^S)^\dagger \psi_{ij}^S, \quad (1)$$

where the pairing interaction is written in an explicit form for the spin-singlet superconductivity with $\psi_{ij}^S =$

$\frac{1}{\sqrt{2}}(c_{i\downarrow}c_{j\uparrow} - c_{i\uparrow}c_{j\downarrow})$ and the strength $V > 0$, which may be directly derived from an antiferromagnetic spin-density interaction or an attractive charge-density interaction between nearest-neighbor sites⁷⁴. To decouple the pairing interaction, we apply the Hubbard-Stratonovich transformation and introduce the auxiliary field Δ_{ij} ⁷⁵:

$$-V\bar{\psi}_{ij}^S\psi_{ij}^S \rightarrow \sqrt{2}(\bar{\Delta}_{ij}\psi_{ij}^S + \bar{\psi}_{ij}^S\Delta_{ij}) + \frac{2|\Delta_{ij}|^2}{V}. \quad (2)$$

The model is generally unsolvable. To proceed, we further adopt a static approximation and ignore the imaginary time dependence of the auxiliary fields. This allows us to integrate out the fermionic degrees of freedom and simulate solely the pairing fields Δ_{ij} . We obtain an effective action:

$$S_{\text{eff}}(\Delta) = -\sum_i \ln(1 + e^{-\beta\Lambda_i}) + \frac{2\beta}{V} \sum_{\langle ij \rangle} |\Delta_{ij}|^2, \quad (3)$$

where β is the inverse temperature and Λ_i are the eigenvalues of the matrix

$$O = \begin{pmatrix} -\mu - T & M \\ M^* & \mu + T \end{pmatrix}, \quad (4)$$

in which T is the $N \times N$ hopping matrix (N is the site number) and $M_{ij} = \Delta_{ij}$ comes from the pairing term.

For spin-singlet pairing, Δ_{ij} is symmetric and defined on the bond between two nearest-neighbor sites ij . We thus have totally $2N$ independent complex variables satisfying the probabilistic distribution:

$$p(\Delta) = Z^{-1}e^{-S_{\text{eff}}}, \quad Z = \int \mathcal{D}\Delta \mathcal{D}\bar{\Delta} e^{-S_{\text{eff}}}, \quad (5)$$

where Z is the partition function serving as the normalization factor. Because O is an Hermitian matrix, all its eigenvalues Λ_i and consequently S_{eff} are real. Hence, the above model can be simulated using Monte Carlo with the Metropolis algorithm. In the following, all presented results are obtained on a 10×10 square lattice ($N = 100$). We have also performed calculations on a 12×12 lattice, and the results are qualitatively consistent. Unfortunately, due to computational limitations, we cannot go to a larger size and conduct a comprehensive finite-size scaling analysis to obtain more accurate transition temperatures. But the qualitative physics is insensitive to the lattice size, and our method is also verified for the standard XY model. For simplicity, only the nearest-neighbor (t) and next-nearest-neighbor (t') hopping parameters are included. We take $t' = -0.45t$ following the common choice in the literature^{76,77} and set t as the energy unit. For real materials, t is typically of the order of 0.1 eV. The chemical potential μ is specially chosen to be -1.4. As plotted in the inset of Fig. 1(a), the corresponding noninteracting dispersion always gives a large Fermi surface as in overdoped cuprates^{78,79}.

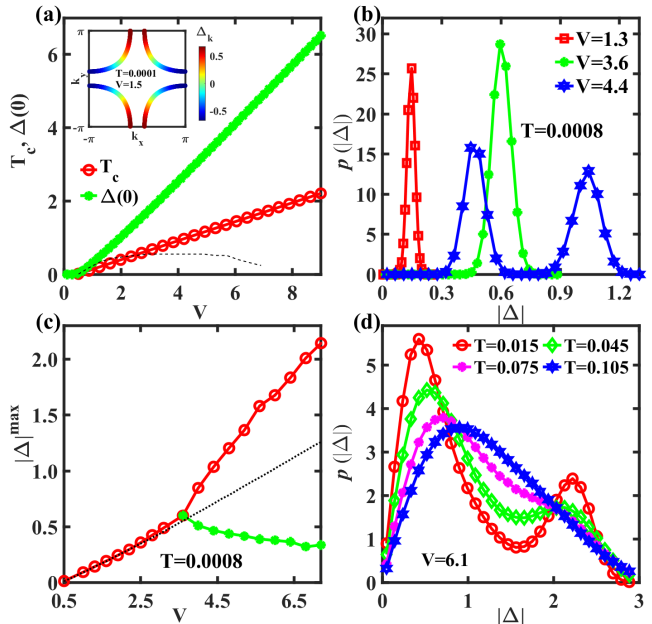


FIG. 1: (a) The mean-field phase diagram, where T_c and $\Delta(0)$ are the superconducting transition temperature and the maximum of the momentum-dependent gap at $T = 0$, respectively. For comparison, the dashed line gives the values of $8T_c$ from our static auxiliary field Monte Carlo simulations to be discussed later. The inset gives the superconducting gap $\Delta_{\mathbf{k}}$ along the Fermi surface for $V = 1.5$ at $T = 0.0001$. (b) Evolution of the amplitude distribution $p(|\Delta|)$ for all bonds at $T = 0.0008$, showing one peak for moderate interaction and two peaks for strong interaction. (c) The peak position $|\Delta|^{\text{max}}$ of $p(|\Delta|)$ as a function of the pairing interaction V , where two maxima are seen to occur for $V \geq 4$. The dotted line shows the uniform mean-field solution for comparison. (d) Evolution of $p(|\Delta|)$ from two-peak to one-peak structure with increasing temperature for $V = 6.1$.

III. RESULTS

For comparison, we first discuss the uniform mean-field solution. The pairing fields are found to satisfy $\Delta^x = -\Delta^y$, where the superscript represents the bond direction. A gap along the Fermi surface is shown in the inset of Fig. 1(a), reflecting a typical $d_{x^2-y^2}$ -wave structure⁸⁰. The maximum gap size $\Delta(T = 0)$ and T_c are plotted in Fig. 1(a) and both increase with increasing pairing interaction V . The typical BCS formula of T_c is reproduced only at small V but violated for $V > 0.5$, where we find a roughly linear relation $T_c \sim V$ with the ratio $2\Delta(0)/T_c \approx 4.6 - 6.1$, which differs from the predictions of the weak-coupling BCS theory. A significant reduction of T_c (dashed line) is found once superconducting fluctuations are included.

A. Spatial correlations of the pairing fields

Our Monte Carlo simulations of the auxiliary pairing fields allow us to study the effect of superconducting fluctuations beyond the mean-field solution. Figure 1(b) shows the amplitude distribution of the pairing field $p(|\Delta|)$ on all bonds at a very low temperature $T = 0.0008$. We focus on moderate and large pairing interactions where T_c is not too small for our numerical simulations. For $V = 1.3$ and 3.6 , the distributions are quite normal and can be well fitted by a Gaussian form. But for $V \geq 4$, it develops a two-peak structure. Figure 1(c) summarizes the peak positions as a function of V for $T = 0.0008$. Compared to the uniform mean-field solution (dotted line), a transition occurs at $V \approx 4.0$, separating the superconductivity into two regions. We will see that they correspond to a homogeneous superconducting state for moderate V and a spatially modulated state for large V , respectively. In Fig. 1(d), the two-peak distribution at large V is gradually suppressed with increasing temperature and becomes a single peak at sufficiently high temperatures. Apart from this, however, the amplitude distribution seems to lack distinctive features in its temperature evolution. We therefore explore mainly the phase fluctuations in the following sections.

We first focus on the homogeneous state for moderate V and study its properties from the perspective of phase correlations of the pairing fields. Our tool is the joint distribution $p(\theta_{\mathbf{0}}^i, \theta_{\mathbf{R}}^i)$, where $\mathbf{0} \equiv (0, 0)$ denotes the bond attached to any origin site, \mathbf{R} represents the relative coordinate of the other bond, and $i = x, y$ denotes the bond along the x - or y -direction. Figure 2(a) plots some typical results for $i = x$ and $\mathbf{R} = (1, 0)$ (short-distance) and $(5, 5)$ (long-distance) at different temperatures. Due to rotational symmetries, the results are the same for $i = y$. At high temperatures, we find a uniform distribution due to strong thermal fluctuations. With lowering temperature, two phases are gradually locked, as manifested by the maximum distribution along the diagonal. A direct comparison shows that this feature first appears on short range with $\mathbf{R} = (1, 0)$ and then on long range with $\mathbf{R} = (5, 5)$. Hence, the phase coherence of the superconducting pairing grows gradually on the lattice to longer distance with decreasing temperature.

To quantify the correlation, we introduce their phase mutual information defined as

$$I_{\mathbf{R}}^i = \int d\theta_{\mathbf{0}}^i d\theta_{\mathbf{R}}^i p(\theta_{\mathbf{0}}^i, \theta_{\mathbf{R}}^i) \ln \frac{p(\theta_{\mathbf{0}}^i, \theta_{\mathbf{R}}^i)}{p(\theta_{\mathbf{0}}^i)p(\theta_{\mathbf{R}}^i)}, \quad (6)$$

where $p(x)$ is the marginal distribution function of the continuous random variable x and $p(x, y)$ is the joint probability distribution of x and y . Figure 2(b) compares the phase correlations as a function of temperature on short and long distances. We see they all exhibit similar behavior below $T_c = 0.054$ and vary exponentially (dashed lines) with the temperature. But for $\mathbf{R} = (5, 5)$, the mutual information suffers from an abrupt change in its temperature dependence and diminishes more rapidly

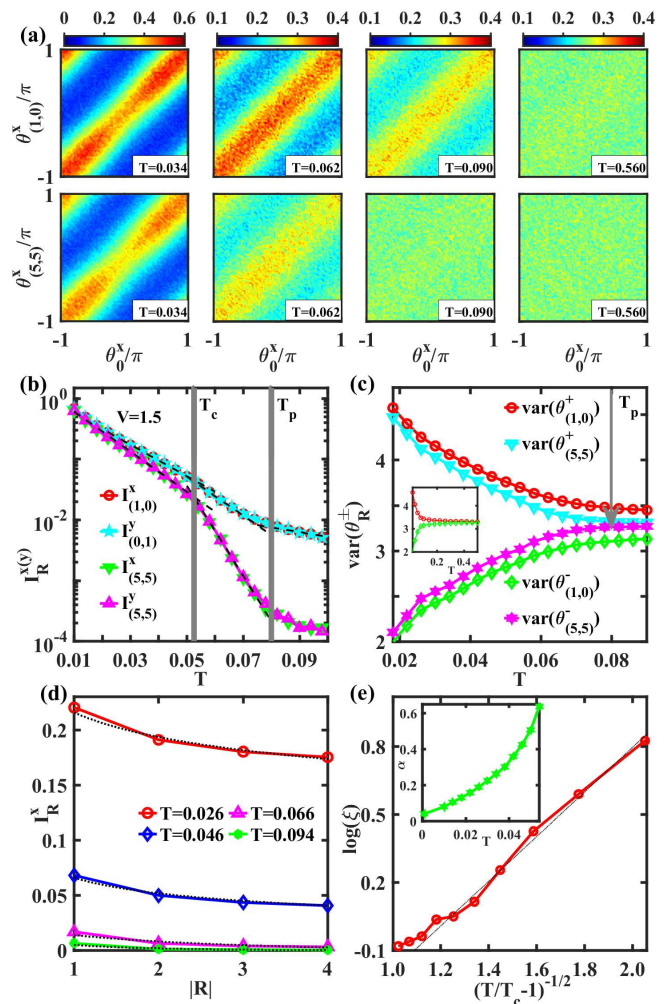


FIG. 2: (a) Comparison of the joint distribution $p(\theta_{\mathbf{0}}^i, \theta_{\mathbf{R}}^i)$ for $\mathbf{R} = (1, 0)$ and $\mathbf{R} = (5, 5)$ at different temperatures. (b) Evolution of the short- and long-distance phase mutual information calculated from (a) as a function of temperature, showing two temperature scales T_c and T_p (vertical grey lines) from the slope change. (c) Temperature dependence of the variance of two principal components $\theta_{\mathbf{R}}^{\pm} = \frac{1}{\sqrt{2}}(\theta_{\mathbf{0}} \pm \theta_{\mathbf{R}})$ from PCA analyses of the data in (a) for short- and long-distance phase correlations. The inset shows the results for $\mathbf{R} = (1, 0)$ on a larger temperature window. (d) Decay of the phase mutual information $I_{\mathbf{R}}^x$ with distance $|\mathbf{R}| = |R_x| + |R_y|$. The dotted lines give the power-law fit using $I_{\mathbf{R}}^x \propto |\mathbf{R}|^{-\alpha}$ below T_c and the exponential fit $I_{\mathbf{R}}^x \propto \exp(-|\mathbf{R}|/\xi)$ above T_c , respectively. (e) The extracted correlation length ξ versus $(T/T_c - 1)^{-1/2}$ following the BKT prediction (dashed line) for $T > T_c$. The inset shows the extracted exponent α for $T < T_c$.

above T_c . Such a slope change actually occurs in the phase mutual information at all distances, but is responsible for the deviation of the phase mutual information at different but close $|\mathbf{R}|$ due to its more rapidly decay with distance above T_c . Thus, T_c marks a characteristic temperature scale separating the phase coherence on different spatial scales, above which long-range correlations

are more rapidly suppressed.

At higher temperature $T_p = 0.08$ for the chosen parameters, a weaker slope change is found for both short- and long-distance correlations. To see what happens at this temperature, we apply the principal component analysis (PCA) to the Monte Carlo samples as collected in Fig. 2(a). As expected, this reveals two principal directions $\theta_{\mathbf{R}}^{\pm} = \frac{1}{\sqrt{2}}(\theta_0 \pm \theta_{\mathbf{R}})$ on the $(\theta_0, \theta_{\mathbf{R}})$ plane for all temperatures, with opposite temperature dependence of their variances. The superscript i is dropped because the data on both bond directions $i = x, y$ are considered together. As shown in Fig. 2(c), the decrease of $\text{var}(\theta_{\mathbf{R}}^-)$ signifies the increase of phase locking degree on the distance \mathbf{R} with lowering temperature. Interestingly, $\text{var}(\theta_{\mathbf{R}}^{\pm})$ become almost equal above T_p along both directions for $\mathbf{R} = (5, 5)$, implying a uniform distribution on the $(\theta_0, \theta_{\mathbf{R}})$ plane and hence the almost complete loss of phase correlation on long distances. On the other hand, the two variances still differ for $\mathbf{R} = (1, 0)$, indicating the existence of short-range correlation. The latter is to be suppressed only at much higher temperatures above $T_l = 0.25$, as shown in the inset of Fig. 2(c). Thus, T_l marks a temperature scale above which no phase correlations are present (a disordered state). Below T_l , the pairing fields start to develop phase correlations between neighboring bonds, indicating the onset of local pairing only. Phase correlations on longer distances only emerge below T_p in the phase fluctuating state and eventually grow into a quasi-long-range order [two-dimensional (2D) superconductivity] at T_c .

The above separation of different regions may be seen from a different angle by plotting the mutual information as a function of the “distance” $|\mathbf{R}| \equiv |R_x| + |R_y|$ (not the Euclidean distance). The results of $I_{\mathbf{R}}^x$ are shown in Fig. 2(d). We observe power-law decay below T_c , characterized by $I_{\mathbf{R}}^x \propto |\mathbf{R}|^{-\alpha}$, while above T_c , the data can be fitted with an exponential function, $I_{\mathbf{R}}^x \propto \exp(-|\mathbf{R}|/\xi)$. The data saturate for larger distances below T_c , reflecting the quasi-long-range order under finite lattice size. We have examined these different behaviors in the standard XY model with the famous Berezinskii-Kosterlitz-Thouless (BKT) transition^{81–83}. A slight difference is that, the finite size effect seems less pronounced in the XY model, possibly due to the inclusion of long-range interactions beyond nearest neighbors by integrating out the fermions in our model. Although finite-size effects cut off the power-law decay with distance below T_c , the temperature dependence of the phase mutual information still effectively captures the transition point for both models. Interestingly, the extracted correlation length ξ also follows closely the scaling, $\log(\xi) \propto (T/T_c - 1)^{-1/2}$, predicted by the BKT transition, and deviates above the phase fluctuation transition temperature T_p . Below T_c , the decay rate α extracted from the power-law scaling of $I_{\mathbf{R}}^x$ decreases with temperature. As shown in the inset, it remains a small value and approaches zero as $T \rightarrow 0$, indicating the establishment of true long-range order in the limit of zero temperature.

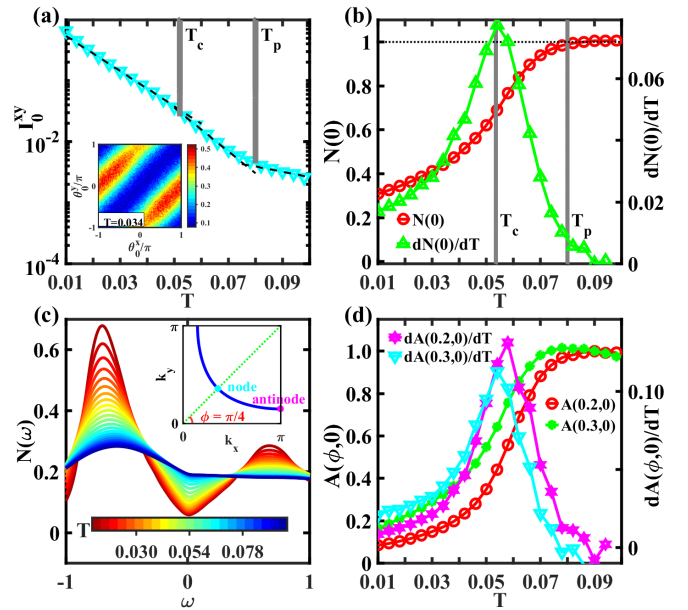


FIG. 3: (a) Temperature dependence of the phase mutual information I_0^{xy} between the x - and y -bonds attached to the same site. The inset shows their joint phase distribution at $T = 0.034$, indicating d -wave correlations between two bonds. (b) The normalized total density of states $N(0)$ at the Fermi energy and its temperature derivative $dN(0)/dT$ as functions of temperature, showing features at T_c and T_p (grey vertical lines) determined from the phase mutual information. (c) Temperature evolution of the total density of states $N(\omega)$, showing the gradual gap opening near the Fermi energy. The inset illustrates the azimuthal angle ϕ and the positions of node and antinode. (d) Temperature dependence of the angle-resolved spectral function $A(\phi, 0)$ and its derivative $dA(\phi, 0)/dT$ at the noninteracting Fermi wave vector and the Fermi energy at $V = 1.5$ for $\phi = 0.2, 0.3$.

B. Effects on spectroscopic properties

Having established how the superconductivity is developed from its phase correlation, we now examine how these may be related to the experimental observations in real materials. First of all, the d -wave nature of the superconducting pairing can be seen from the joint distribution of θ_0^x and θ_0^y connected to the same site. As shown in the inset of Fig. 3(a), we find a rough correlation, $\theta_0^y = \theta_0^x \pm \pi$, namely a sign change of the pairing fields along two perpendicular bond directions. Here we define the mutual information between θ_0^x and θ_0^y attached to the same site along two perpendicular directions:

$$I_0^{xy} = \int d\theta_0^x d\theta_0^y p(\theta_0^x, \theta_0^y) \ln \frac{p(\theta_0^x, \theta_0^y)}{p(\theta_0^x)p(\theta_0^y)}. \quad (7)$$

As we can see in Fig. 3(a), its temperature dependence exhibits similar slope changes at T_c and T_p .

The separation of phase correlations on short and long distances has important consequences on the spectral

properties, which may be studied by assuming a twist boundary condition to overcome the finite-size effect⁸⁴. Figure 3(b) plots the total density of states at the Fermi energy $N(0)$ normalized by its high-temperature value. It is almost a constant above T_p , but then decreases gradually with lowering temperature, reflecting the spectral weight depression induced by a gap opening at zero energy. Interestingly, its temperature derivative $dN(0)/dT$ exhibits a maximum at around T_c , consistent with the slope change of the phase mutual information $I_{(5,5)}^{x(y)}$. Correspondingly, as shown in Fig. 3(c), a pseudogap develops gradually on $N(\omega)$ with lowering temperature over the intermediate range $T_c < T < T_p$. These establish a close relation between the phase correlation and the spectral gap of the superconductivity.

A similar temperature evolution is also seen in the angle-resolved spectral function $A(\phi, 0)$ and its temperature derivative $dA(\phi, 0)/dT$ along the azimuthal angle ϕ at the noninteracting Fermi wave vector and zero energy. For larger ϕ away from the antinode, the spectral function grows to a maximum at lower temperature and has a higher residual value at the zero-temperature limit. Meanwhile, its temperature derivative becomes more enhanced below T_c but suppressed above T_c . Such an intrinsic anisotropy has been observed in the latest ARPES experiment⁴⁵.

To clarify the origin of the anisotropy, we compare in Fig. 4(a) the temperature dependence of the spectral functions $A(\phi, \omega)$ for different azimuthal angle ϕ . Obviously, they exhibit very different behaviors near nodal or antinodal directions. Figure 4(b) plots the extracted spectral gap $\Delta(\phi, T)$ as a function of temperature. With increasing temperature, the gap closes first near the nodal direction. Thus as shown in Fig. 4(c), it only satisfies the ideal d -wave form $\Delta(\phi, T) \propto \cos(2\phi)$ (green dashed line) at sufficiently low temperatures. This is beyond the mean-field approximation but reflects the effect of phase fluctuations. Consequently, the scattering rate $\Gamma(\phi)$ estimated from the half-maximum half-width of the upper peak of $A(\phi, \omega)$ also exhibits smaller values near the node.

The anisotropy of the spectral functions has an effect on the angle-resolved thermal entropy $S(\phi, T)$ and the specific heat coefficient $\gamma(\phi, T) = dS(\phi, T)/dT$ by using $S(\phi, T) = -\int d\omega A(\phi, \omega)[f \ln f + (1-f) \ln(1-f)]$, where f is the Fermi distribution function. As shown in Figs. 4(d) and 4(e), the resulting $S(\phi, T)$ and $\gamma(\phi, T)$ exhibit similar temperature and angle dependence to $A(\phi, 0)$ and $dA(\phi, 0)/dT$ in Fig. 3(d), which agree well with the entropy reduction and specific-heat anisotropy reported in the latest ARPES experiment⁴⁵.

To further compare with experiment⁴⁵, Fig. 5(a) plots the energy-momentum dependent spectral function $A(k_y, E)$ at fixed $k_x = -3.047$, which allows us to extract the energy of the maxima for each k_y . The resulting dispersions are shown in Fig. 5(b) for $T = 0.098, 0.07, 0.022$. We see that the dispersion exhibits back bending even for $T = 0.07 > T_c$ but almost recovers the normal state one

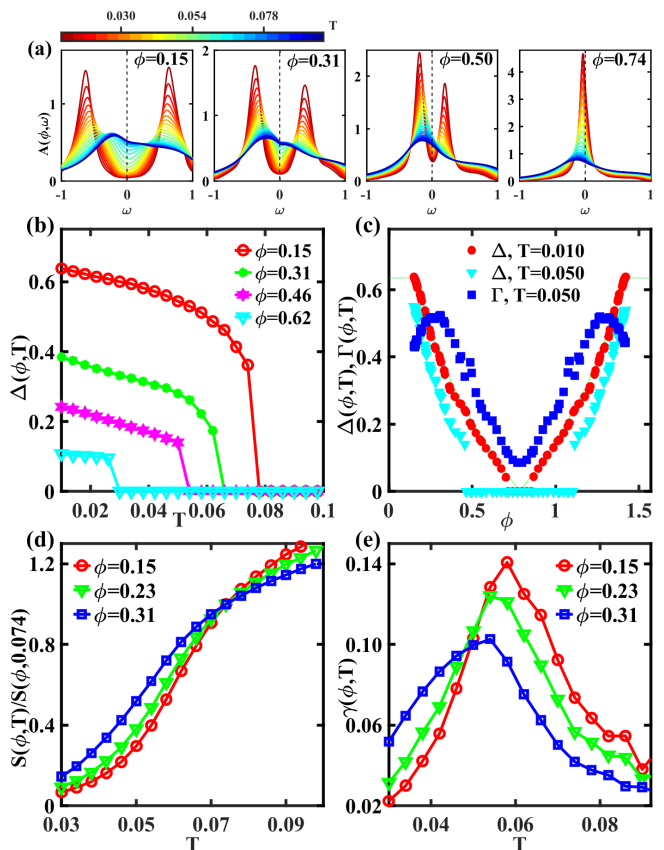


FIG. 4: (a) Temperature evolution of the angle-resolved spectral function $A(\phi, \omega)$ on different positions of the Fermi surface. (b) Comparison of the extracted gap $\Delta(\phi, T)$ from (a) as functions of the temperature T . (c) Angular dependence of the spectral gap $\Delta(\phi, T)$ and scattering rate $\Gamma(\phi, T)$ on the Fermi surface. Δ and Γ are defined as the energy and the half-maximum half-width of the upper peak of the spectral function $A(\phi, \omega)$. (d) and (e) give the calculated thermal entropy $S(\phi, T)$ and specific heat coefficient $\gamma(\phi, T)$ as functions of temperature at different positions (ϕ) on the Fermi surface.

for $T = 0.098 > T_p$. The vector k_G where the bending occurs is the same as the Fermi vector $k_F = \pm 0.4712$ (the gray vertical line), which differs from the prediction based on density wave or magnetic order pictures. The extracted dispersion also manifests anisotropy due to phase fluctuations. In Fig. 5(c), the dispersion near k_F (the gray vertical line) shows an angle-dependent gap at $T = 0.034$, but a clear node-antinode dichotomy at $T = 0.066$, with the near-node dispersion crossing the Fermi energy and the near-antinode dispersion exhibiting a gap and back bending, as reported previously in underdoped experiments¹⁵.

The effect of the phase correlation is also reflected in the topology of the Fermi surface. As shown in the inset of Fig. 5(d), the angle-dependent spectral function $A(\phi, 0)$ is gradually suppressed away from the nodal point with lowering temperature. This leads to a variation of

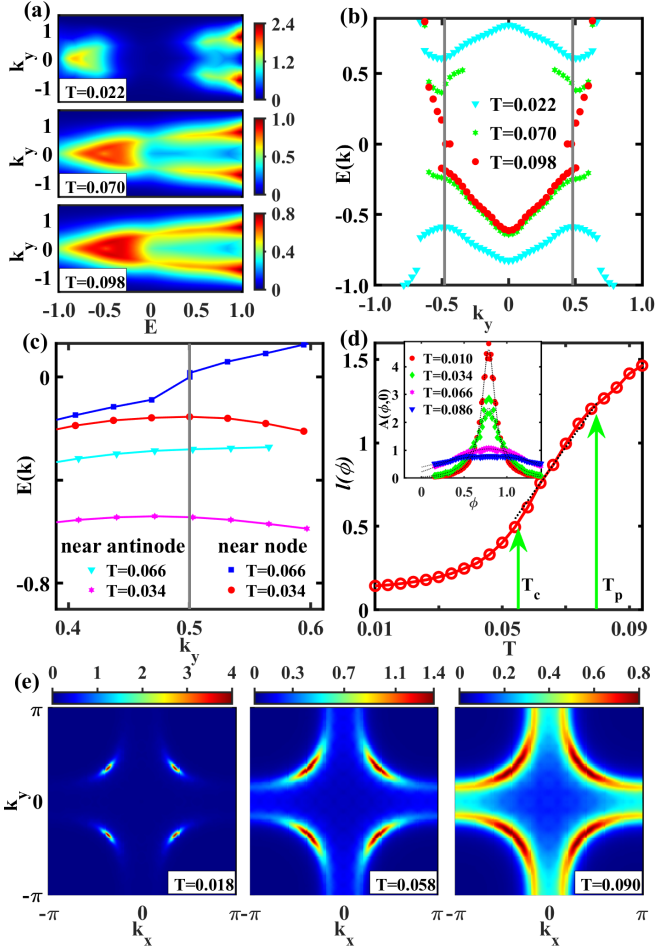


FIG. 5: (a) Intensity plot of the spectral function $A(k_y, \omega)$ for $k_x = -3.047$ at $T = 0.022, 0.070, 0.098$. (b) Extracted dispersions from the spectral functions at different temperatures, showing back bending even above T_c . The vertical grey lines mark the Fermi wave vector $k_y = \pm 0.4712$. (c) The dispersions near antinode and node for $T = 0.066$ and 0.034 . For comparison, all curves are shifted such that the Fermi wave vectors are located at $k_y = 0.5$ (grey line). For clarity, only the lower (negative energy) parts of the superconducting dispersions are shown. (d) Length of the Fermi arc $l(\phi)$ as a function of temperature. The green arrows mark T_c and T_p , and the dashed line is a guide to the eye. The inset shows Lorentzian fit of the angle-dependent spectral function $A(\phi, 0)$ on the Fermi surface. (e) Intensity plot of the spectral function $A(\mathbf{k}, 0)$ at zero energy in the first Brillouin zone for different temperatures, showing gradual development of the Fermi arc.

the Fermi arc^{27,85,86}, whose length $l(\phi)$, estimated from the 0.6-maximum width of the spectral peak, is plotted in Fig. 5(d) as a function of temperature. We see that $l(\phi)$ almost saturates below T_c , increases linearly with temperature in the intermediate region, and reaches a full length (Fermi surface) at high temperatures. This confirms its connection with the phase correlation identified using the phase mutual information. Such a tempera-

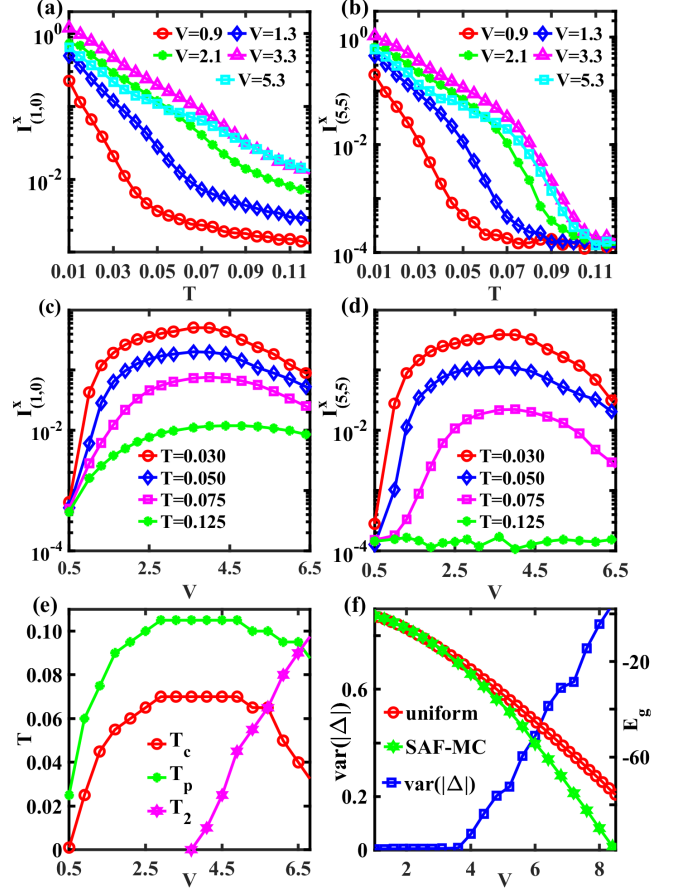


FIG. 6: Comparison of the short- and long-distance phase mutual information with $\mathbf{R} = (1, 0)$ and $(5, 5)$ (a)(b) as functions of temperature for different pairing interactions, and (c)(d) as functions of the pairing interactions for different temperatures. (e) The superconducting phase diagram with T_c and T_p determined from the phase mutual information and T_2 from the onset of two-peak amplitude distribution. (f) Comparison of the condensation energy E_g for the uniform mean-field solution and the static auxiliary field Monte Carlo (SAF-MC) solution. Also shown in the variance of the amplitude distribution $\text{var}(|\Delta|)$ from the Monte Carlo simulations at $T = 0.001$.

ture variation of the Fermi arc length has been observed in scanning tunneling spectroscopy (STS) experiment²⁰, implying that the zero arc length reported in the ARPES experiments⁸⁷ might originate from the peaks of the artificially symmetrized $A(\phi, \omega)$. To be specific, Fig. 5(e) maps out the zero-energy spectral function $A(\mathbf{k}, 0)$ in the first Brillouin zone, and we see a clear evolution from the Fermi arc at $T = 0.058$ to the Fermi surface $T = 0.09$. This variation indicates that the Bogoliubov quasiparticle appears at different temperatures in different regions of the Fermi surfaces. The arc is more broadened close to the node, consistent with previous experiment⁸⁸.

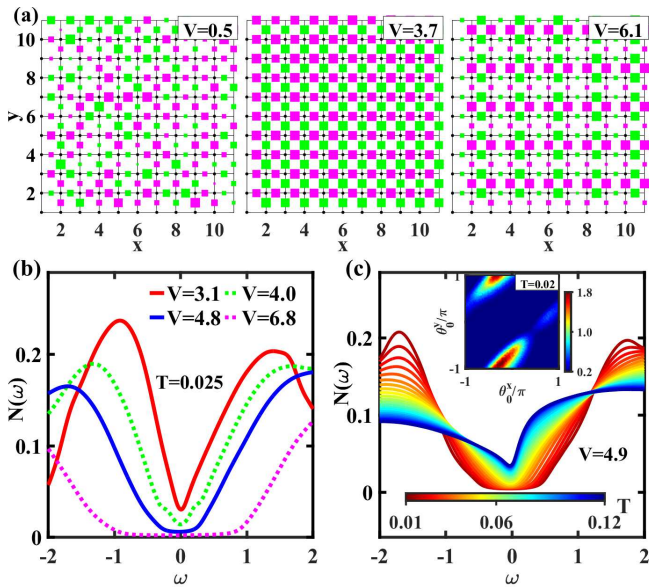


FIG. 7: (a) Typical configurations of the pairing fields at $T = 0.001$ for $V = 0.5, 3.7, 6.1$. The square size represents their amplitude and the colors mark the sign of their phase $\theta \in (-\pi, \pi]$. (b) Evolution of the total density of state $N(\omega)$ with pairing interactions at $T = 0.025$, showing a crossover from V-shape to U-shape. (c) Temperature dependence of $N(\omega)$ at $V = 4.9$. The inset shows the joint distribution of θ_0^x and θ_0^y at $T = 0.02$, indicating d -wave-like bonds for the pairing fields in the plaquette state.

C. The superconducting phase diagram and a strong-coupling plaquette state

Having identified the different regions of phase correlations at a fixed V , we now turn to their variation with the pairing interaction. As shown in Figs. 6(a) and 6(b), the range of exponential temperature dependence also varies. As V increases, the curves first move to higher temperatures, but then shift somewhat backwards. Such a non-monotonic variation is better seen in Figs. 6(c) and 6(d), where the phase mutual information $I_{(1,0)}^x$ and $I_{(5,5)}^x$ are replotted as a function of V for different temperatures. Both exhibit nonmonotonic behavior with increasing V at low temperatures, indicating that the phase correlations are suppressed when the pairing interaction is getting too large. As we will see, this is closely associated with the two-peak structure of the amplitude distribution in Fig. 1(d).

Taken together, a superconducting phase diagram can be constructed and shown in Fig. 6(e), where both T_c and T_p behave nonmonotonically with V . Also shown is a third temperature scale T_2 , below which the amplitude distribution has two peaks. T_2 only appears for sufficiently large V , indicating a strong coupling limit whose nature will be clarified later. Interestingly, we see that T_c takes its maximum near the critical V of the two-peak distribution and is suppressed as T_2 increases. This sug-

gests that the superconductivity is competing with this strong coupling state.

To clarify this issue, we compare in Fig. 7(a) typical Monte Carlo configurations of the pairing fields for weak, intermediate, and strong V at $T = 0.001$. The size of the square represents the amplitude $|\Delta|$ and the color denotes the sign of the phase $\theta \in (-\pi, \pi]$. For weak $V = 0.5$, the distribution on the lattice is random, reflecting that the system is not yet in a phase-coherent region ($T > T_c$). For intermediate $V = 3.7$, we find a uniform distribution of the amplitude, while the phase changes sign periodically and exhibits a d -wave-like pattern. It is straightforward to identify this state as the uniform d -wave superconductivity. For strong $V = 6.1$, the amplitude distribution is no longer uniform but exhibits cluster patterns. We call it a charge- $4e$ d -wave plaquette state since it is formed out of local plaquettes⁸⁹ with four bonds of large $|\Delta|$ in a unit cell surrounded by weak bonds in a 2×2 cell. The plaquette has the same sign structure as the d -wave superconductivity. The whole state can be regarded as weakly connected charge- $4e$ plaquettes. Clearly, this is not a phase separation and the two-peak feature of the amplitude distribution is a reflection of the special plaquette structure. This state breaks the translational invariance of the pairing fields, but keeps the uniform distribution of the electron densities. It persists to a very large $V = 7.5$, beyond which the bonds become less correlated as $t/V \rightarrow 0$.

To show that the plaquette state is stable over the uniform superconductivity, we calculate their condensation energies using

$$E_g = \sum_l |\xi_l| + \sum_{\langle ij \rangle} \frac{2|\Delta_{ij}|^2}{V} - \sum_l \Lambda_l, \quad (8)$$

where $l = 1, 2, \dots, N$ and ξ_l is the eigenvalue of the non-interacting Hamiltonian. Figure 6(f) compares the condensation energies of the mean-field uniform solution and the Monte Carlo solution. For small V , we see they are almost equal. But beyond the critical V of the plaquette state, the mean-field uniform solution has higher energy than the Monte Carlo (plaquette) solution. In this region, the variance $\text{var}(|\Delta|)$ of the amplitude distribution grows rapidly with increasing V , reflecting an increasing difference between the strong and weak bonds.

The transition to the plaquette state may be detected from the V-shape-to-U-shape change of the density of states as shown in Fig. 7(b). Figure 7(c) plots $N(\omega)$ at $V = 4.9$ for different temperatures. The plaquette state melts as $N(\omega)$ changes from U-shape to V-shape with increasing temperature. Note that a U-shaped curve is typically ascribed to s -wave superconductivity. However, the plaquette state still exhibits d -wave-like bonds as shown in the inset of Fig. 7(c). A similar variation has been observed in STS measurement in twisted trilayer graphene⁷³, where it was argued to originate from two-particle bound states. In our simulations, the four-particle plaquette state is more favored with nearest-neighbour pairing interaction.

It has been suggested that strong attractive interaction may always lead to phase separation⁹⁰⁻⁹⁴. It could be that the pairing interaction for the plaquette state is not yet strong enough. For sufficiently large V , we find randomly distributed dimers and plaquettes, possibly because the pairing correlations are suppressed as t/V becomes too small. The plaquette state may be in some sense related to a pair density wave (PDW)⁹⁵⁻⁹⁷. But our derived configuration is special. It does not induce any charge-density wave and may only be produced by a complicated combination of uniform superconductivity and bidirectional PDW states of the wave vector $(0, \pi)$ and $(\pi, 0)$. It may thus be better viewed as a different strong-coupling limit of the d -wave superconductivity.

IV. DISCUSSION AND CONCLUSIONS

We have applied the static auxiliary field Monte Carlo method to study phase correlations of the superconducting pairing fields. We can reproduce the weak-coupling BCS solution of the mean-field theory and identify a region above T_c by separation between short- and long-distance phase correlations for moderate and strong pairing interactions. This phase fluctuating region above the uniform d -wave superconductivity has a number of spectroscopic features including the anisotropy of the angle-resolved gap opening, scattering rate, and specific heat coefficient, as well as gradual development of the Fermi arc. These provide a potential explanation of the experimental observations in overdoped cuprates, and suggest that angular or momentum dependence of the gap opening temperature may be a general feature of phase fluctuations. For sufficiently strong pairing interaction, our simulation reveals a competing charge- $4e$ plaquette state with d -wave-like bonds and a U-shaped density of states, which may be useful for understanding the pairing in strong coupling limit. The superconducting transition temperature seems maximal near the critical pairing interaction of the plaquette state, raising an interesting question concerning their relationship.

While our method captures the superconducting fluctuations at finite temperatures beyond the uniform mean-field theory, it ignores the imaginary-time dependence of the pairing fields and therefore cannot apply at very low temperatures where quantum fluctuations become important. By integrating out the fermions, we only focus on the superconducting properties where nearest-neighbor pairing plays a dominant role. It should be mentioned that we begin the calculations with an attractive spin-singlet pairing interaction. Ignoring other possible instabilities, this effective pairing interaction covers a variety of microscopic pairing mechanisms, including the nearest-neighbor antiferromagnetic spin interaction, the nearest-neighbor attractive charge density interaction⁹⁸⁻¹⁰⁰, and the spin fluctuation mechanism in momentum space⁷⁴. While these mechanisms may be supported by different experiments^{98,101,102}, they exhibit

similar superconducting properties as revealed in our calculations.

It may be useful to compare our results of the uniform superconductivity with the XY model which is believed to describe the physics of two-dimensional superconductivity^{10,12,103}. For this purpose, we have to first define the superconducting order parameter on the lattice sites, namely $\Delta_i = \frac{1}{4}(\Delta_{i,i+x} + \Delta_{i,i-x} - \Delta_{i,i+y} - \Delta_{i,i-y})$, where $\Delta_{i,i\pm x}$ and $\Delta_{i,i\pm y}$ are the pairing fields on the four bonds connected to site i . The number of vortices can then be calculated using Δ_i following the standard definition¹³ and found to be nearly zero below T_c , grow rapidly between T_c and T_p and slowly above T_p , and eventually saturate above T_l . The rapid increase above T_c is in good correspondence with that predicted for the BKT transition due to the unbinding of vortices and antivortices, indicating that our T_c is exactly the BKT transition temperature. The power law decay of the phase mutual information indicates a quasi-long range order that does not break U(1) symmetry conforming to the well-known Mermin-Wagner theorem^{104,105}. Our identification of three temperature scales and four distinct regions may offer some insight into the triple transition in resistance experiment⁴¹, where normal metal, pseudogap (incoherent metal), phase fluctuation, and superconductivity are separated. A similar scenario may also be related to the transition between superconductivity and normal metal, where disorder or magnetic field may broaden the transition and lead to one or two intermediate regions^{106,107}.

Superconducting phase fluctuations also play an important role in other superconductors, such as Fe-based superconductors¹⁰⁸⁻¹¹¹ and disordered conventional superconductors¹¹²⁻¹¹⁸. Our method may also provide useful insight into the interplay between phase fluctuations and other important effects such as disorder, multiband, and time reversal symmetry breaking in these systems.

This work was supported by the National Natural Science Foundation of China (NSFC Grants No. 11974397, No. 12174429, and No. 12204075), the National Key Research and Development Program of China (Grant No. 2022YFA1402203), and the Strategic Priority Research Program of the Chinese Academy of Sciences (Grant No. XDB33010100).

Appendix A: ORIGIN OF THE PAIRING INTERACTION

We show that the spin singlet pairing interaction may be derived from different microscopic models. To see this, we first define the spin-singlet and spin-triplet pairing

operators in real space:

$$\begin{aligned}\psi_{ij}^S &= \frac{1}{\sqrt{2}} \sum_{\alpha,\beta} c_{i\alpha} (-i\sigma_y)_{\alpha\beta} c_{j\beta}, \\ \psi_{ij}^T &= \frac{1}{\sqrt{2}} \sum_{\alpha,\beta} c_{i\alpha} (-i\sigma_y \boldsymbol{\sigma})_{\alpha\beta} c_{j\beta},\end{aligned}\quad (\text{A1})$$

which satisfy $\psi_{ji}^S = \psi_{ij}^S$ and $\psi_{ji}^T = -\psi_{ij}^T$.

For nearest-neighbor attractive charge density interaction, we have

$$\begin{aligned}V_{\text{int}} &= -V^c \sum_{\langle ij \rangle} n_i n_j \\ &= -V^c \sum_{\langle ij \rangle} \left[(\psi_{ij}^S)^\dagger \psi_{ij}^S + (\psi_{ij}^T)^\dagger \psi_{ij}^T \right].\end{aligned}\quad (\text{A2})$$

Since this model favors d -wave superconductivity^{35,99}, we may discard the spin-triplet part and obtain the singlet pairing interaction in Eq. (1) with $V = V^c$.

For nearest-neighbor antiferromagnetic spin density interaction, we have

$$\begin{aligned}V_{\text{int}} &= \sum_{\langle ij \rangle} J \mathbf{s}_i \cdot \mathbf{s}_j \\ &= -\frac{J}{4} \sum_{\langle ij \rangle} \left[3 (\psi_{ij}^S)^\dagger \psi_{ij}^S - (\psi_{ij}^T)^\dagger \psi_{ij}^T \right].\end{aligned}\quad (\text{A3})$$

Again, we may exclude the spin-triplet pairing and obtain the singlet pairing interaction in Eq. (1) with $V = \frac{3}{4}J$.

The spin fluctuation interaction in momentum space may be transformed into real space, yielding

$$V_{\text{int}} = \sum_{\mathbf{q}} V(\mathbf{q}) \mathbf{s}_{\mathbf{q}} \cdot \mathbf{s}_{-\mathbf{q}} = \sum_{ij} V(\mathbf{r}_i - \mathbf{r}_j) \mathbf{s}_i \cdot \mathbf{s}_j, \quad (\text{A4})$$

where $\mathbf{s}_{\mathbf{q}} = \sum_{\mathbf{k}} \sum_{\alpha,\beta} c_{\mathbf{k}+\mathbf{q}\alpha}^\dagger \frac{\boldsymbol{\sigma}_{\alpha,\beta}}{2} c_{\mathbf{k}\beta}$ and $V(\mathbf{r}_i) = \sum_{\mathbf{q}} V(\mathbf{q}) e^{i\mathbf{q}\mathbf{r}_i}$. For some typical phenomenological form of $V(\mathbf{q})$ ⁷⁶, the deduced interaction in real space is dominated by onsite repulsion interaction and nearest-neighbor antiferromagnetic spin density interaction. Excluding the onsite pairing and considering only the nearest-neighbor pairing yield the singlet pairing interaction in Eq. (1).

Appendix B: THE EFFECTIVE ACTION

The action of the Hamiltonian (1) is

$$\begin{aligned}S[\bar{c}, c] &= \int_0^\beta d\tau \left[\sum_{i\ell\sigma} \bar{c}_{i\sigma}(\tau) ((\partial_\tau - \mu)\delta_{i\ell} - t_{i\ell}) c_{\ell\sigma}(\tau) \right. \\ &\quad \left. - V \sum_{\langle ij \rangle} \bar{\psi}_{ij}^S(\tau) \psi_{ij}^S(\tau) \right].\end{aligned}\quad (\text{B1})$$

To decouple the pairing interaction term, we use the Hubbard-Stratonovich transformation⁷⁵ by introducing the auxiliary pairing field Δ_{ij} for each nearest-neighbor pair:

$$\begin{aligned}-V \bar{\psi}_{ij}^S(\tau) \psi_{ij}^S(\tau) &\rightarrow \\ &\sqrt{2} (\bar{\Delta}_{ij} \psi_{ij}^S(\tau) + \bar{\psi}_{ij}^S(\tau) \Delta_{ij}) + \frac{2|\Delta_{ij}|^2}{V},\end{aligned}\quad (\text{B2})$$

where $\bar{\Delta}_{ij}$ is the complex conjugate of Δ_{ij} . In the static approximation, the pairing fields are assumed to be independent of the imaginary time τ .

We have thus the new action,

$$S = \sum_n \bar{\psi}(i\omega_n) (-i\omega_n + O) \psi(i\omega_n) + \frac{2\beta}{V} \sum_{\langle ij \rangle} |\Delta_{ij}|^2, \quad (\text{B3})$$

where $[\bar{\psi}(i\omega_n)]_j = \bar{c}_{j\uparrow}(i\omega_n)$, $[\bar{\psi}(i\omega_n)]_{N+j} = c_{j\downarrow}(-i\omega_n)$ for $j = 1, 2, \dots, N$, and

$$O = \begin{pmatrix} -\mu - T & M \\ M^* & \mu + T \end{pmatrix}, \quad (\text{B4})$$

in which $T_{ij} = t_{ij}$ is the hopping matrix and $M_{ij} = \Delta_{ij}$ contains the pairing term. Integrating out the fermions yields the final effective action,

$$S_{\text{eff}} = - \sum_i \ln(1 + e^{-\beta\Lambda_i}) + \frac{2\beta}{V} \sum_{\langle ij \rangle} |\Delta_{ij}|^2, \quad (\text{B5})$$

where Λ_i is the eigenvalue of O . In deriving this expression, we have used

$$\int \mathcal{D}\bar{\psi} \mathcal{D}\psi e^{-\sum_n \bar{\psi}(i\omega_n) (-i\omega_n + O) \psi(i\omega_n)} = \prod_n \det(O - i\omega_n), \quad (\text{B6})$$

and

$$\sum_n \ln(\Lambda_i - i\omega_n) e^{i\omega_n 0^+} = \ln(1 + e^{-\beta\Lambda_i}). \quad (\text{B7})$$

Appendix C: THE MEAN FIELD SOLUTION

Under mean-field approximation, we define $\Delta_{ij} = -\frac{1}{\sqrt{2}} V \langle \psi_{ij}^S \rangle$ and assume a uniform mean-field solution $\Delta_{ij}^x = \Delta_x$ and $\Delta_{ij}^y = \Delta_y$ with $\Delta_x = -\Delta_y = \Delta$. This leads to a d -wave gap in the momentum space, $\Delta_{\mathbf{k}} = 2\Delta [\cos(k_x) - \cos(k_y)]$, that satisfies

$$\Delta = \frac{V}{N} \sum_{\mathbf{k}} \frac{\Delta_{\mathbf{k}}}{2E_{\mathbf{k}}} [1 - 2f(E_{\mathbf{k}})] \cos(k_x), \quad (\text{C1})$$

where $f(E_{\mathbf{k}})$ is the Fermi-Dirac distribution function, $E_{\mathbf{k}} = \sqrt{|\Delta_{\mathbf{k}}|^2 + \xi_{\mathbf{k}}^2}$, and $\xi_{\mathbf{k}}$ is the dispersion of an electron.

Appendix D: MONTE CARLO SIMULATIONS

The effective action (B5) gives the probabilistic distribution of the $2N$ independent complex variables Δ_{ij} :

$$p(\Delta) = Z^{-1} e^{-S_{\text{eff}}}, \quad Z = \int \mathcal{D}\Delta \mathcal{D}\bar{\Delta} e^{-S_{\text{eff}}}, \quad (\text{D1})$$

which may be simulated using the Monte Carlo approach with the Metropolis algorithm following the standard procedures:

(a) Assign random initial values to the pairing field, Δ_{ij} , on each bond and calculate the matrix O and its eigenvalues.

(b) Update the pairing field to, $|\Delta_{ij}'| = |\Delta_{ij}| + \eta_a x V$ or $\theta'_{ij} = \theta_{ij} + \eta_t x$, with x being a random number distributed uniformly between -1 and 1. We find that $\eta_a = 1$ and $\eta_t = \pi$ can give an appropriate acceptance rate.

(c) Calculate the change in the effective action, $\delta S = S_{\text{eff}}(\Delta') - S_{\text{eff}}(\Delta)$, and accept the update with probability $\min\{1, \exp(-\delta S)\}$.

(d) Repeat (b) and (c) for 10000 sweeps for thermalization and then 150000 sweeps for measurement. During the measurement, we take one sample for $2N$ pairing fields after every 10 sweeps to reduce the self-correlation effect in the data. All physical quantities are calculated by averaging over 15000 configurations of the pairing fields.

Appendix E: MUTUAL INFORMATION

The mutual information between two continuous random variables X and Y is defined as⁵⁷

$$I(X, Y) = \int \int p(x, y) \log \frac{p(x, y)}{p(x)p(y)} dx dy, \quad (\text{E1})$$

where $p(x, y)$ is their joint probability distribution function, and $p(x)$ and $p(y)$ are their respective marginal probability distribution functions. We have $p(x) = \int p(x, y) dy$ and $p(y) = \int p(x, y) dx$. In practice, we divide the variable domain into intervals and calculate the mutual information by

$$I(X, Y) \approx \sum_{i,j} p_{i,j} \log \frac{p_{i,j}^{xy}}{p_i^x p_j^y}, \quad (\text{E2})$$

where $p_{i,j}^{xy}$, p_i^x , and p_j^y are the probabilities for X and Y taking values in the i -th and j -th intervals, respectively.

We have chosen 21 intervals in our calculations of the phase mutual information. The results are found to be qualitatively stable if we change the interval size within an appropriate range, or adopt other methods including the adaptive interval partition⁵⁹, the KSG method based on k -th nearest neighbors⁵⁸, and the neural network estimation⁶².

Appendix F: SPECTRAL CALCULATIONS

To overcome the finite-size effects for spectral property calculations, we apply the twisted boundary conditions⁸⁴:

$$c_{i\sigma} \rightarrow c_{i\sigma} e^{-i\sigma\phi \cdot \mathbf{r}_i}, \quad \phi = \left(\frac{2\pi l_x}{n_x m_x}, \frac{2\pi l_y}{n_y m_y} \right) \quad (\text{F1})$$

with $l_x = 0, 1, \dots, m_x - 1$ and $l_y = 0, 1, \dots, m_y - 1$. Here m_x (m_y) denotes the number of sublattices in the x (y) direction, and n_x (n_y) denote the number of lattice sites in the x (y) direction of the original lattice. For a square lattice, we have $m_x = m_y$ and $n_x = n_y$. This corresponds to the following transformation:

$$\begin{aligned} t_{ij} &\rightarrow t_{ij} e^{i\phi \cdot \mathbf{r}_i}, & \mu &\rightarrow \mu, \\ \bar{\Delta}_{ij} &\rightarrow \bar{\Delta}_{ij} e^{i\phi \cdot \mathbf{r}_i}, & \Delta_{ij} &\rightarrow \Delta_{ij} e^{i\phi \cdot \mathbf{r}_i}, \end{aligned} \quad (\text{F2})$$

where $\mathbf{r}_l = \mathbf{r}_j - \mathbf{r}_i$.

In momentum space, the dispersion changes to, $\epsilon_{\mathbf{k}} \rightarrow \epsilon_{\mathbf{k}+\phi} = -\sum_{ij} t_{ij} e^{i(\mathbf{k}+\phi) \cdot \mathbf{r}_i}$, which effectively includes $m_x n_x \times m_y n_y$ \mathbf{k} -points for calculating physical properties. The pairing fields are then

$$\Delta_{\mathbf{k}_1+\phi, \mathbf{k}_2+\phi} = \frac{1}{N} \sum_{ij} \Delta_{ij} e^{i\phi \cdot \mathbf{r}_i - i\mathbf{k}_2 \cdot \mathbf{r}_i + i\mathbf{k}_1 \cdot \mathbf{r}_j}. \quad (\text{F3})$$

We have in the action,

$$O = \begin{pmatrix} \epsilon_{\mathbf{k}+\phi} - \mu & M \\ M^\dagger & -\epsilon_{\mathbf{k}+\phi} + \mu \end{pmatrix}, \quad (\text{F4})$$

where $M_{ij} = \Delta_{\mathbf{k}_j+\phi, \mathbf{k}_i+\phi}$. This can be diagonalized for each ϕ and field configuration. The electron Green's function is then obtained after averaging over all field configurations, which gives the spectral function and the density of states presented in the main text.

* yifeng@iphy.ac.cn

¹ V. J. Emery and S. A. Kivelson, Importance of Phase Fluctuations in Superconductors with Small Superfluid Density, *Nature* **374**, 434 (1995).

² M. Franz and A. Millis, Phase fluctuations and spectral properties of underdoped cuprates, *Phys. Rev. B* **58**, 14572 (1998).

³ H. J. Kwon, A. T. Dorsey, and P. J. Hirschfeld, Observability of Quantum Phase Fluctuations in Cuprate Super-

conductors, *Phys. Rev. Lett.* **86**, 3875 (2001).

⁴ K. V. Samokhin and B. Mitrović, Nodal Quasiparticles and Classical Phase Fluctuations in d -Wave Superconductors, *Phys. Rev. Lett.* **92**, 057002 (2004).

⁵ M. R. Norman, A. Kanigel, M. Randeria, U. Chatterjee, and J. C. Campuzano, Modeling the Fermi arc in underdoped cuprates, *Phys. Rev. B* **76**, 174501 (2007).

⁶ E. Berg and E. Altman, Evolution of the Fermi Surface of d -Wave Superconductors in the Presence of Thermal

- Phase Fluctuations, Phys. Rev. Lett. **99**, 247001 (2007).
- ⁷ Z. Tešanović, *d*-Wave Duality and Its Reflections in High-Temperature Superconductors, Nat. Phys. **4**, 408 (2008).
- ⁸ S. Banerjee, T. V. Ramakrishnan, and C. Dasgupta, Effect of pairing fluctuations on low-energy electronic spectra in cuprate superconductors, Phys. Rev. B **84**, 144525 (2011).
- ⁹ A. Allais, D. Chowdhury, and S. Sachdev, Connecting High-Field Quantum Oscillations to Zero-Field Electron Spectral Functions in the Underdoped Cuprates, Nat. Commun. **5**, 5771 (2014).
- ¹⁰ T. Eckl, D. J. Scalapino, E. Arrigoni, and W. Hanke, Pair phase fluctuations and the pseudogap, Phys. Rev. B **66**, 140510(R) (2002).
- ¹¹ M. Mayr, G. Alvarez, C. Şen, and E. Dagotto, Phase Fluctuations in Strongly Coupled *d*-Wave Superconductors, Phys. Rev. Lett. **94**, 217001 (2005).
- ¹² Q. Han, T. Li, and Z. D. Wang, Pseudogap and Fermi-arc evolution in the phase-fluctuation scenario, Phys. Rev. B **82**, 052503 (2010).
- ¹³ Y. W. Zhong, T. Li, and Q. Han, Monte Carlo Study of thermal fluctuations and Fermi-arc formation in *d*-wave superconductors, Phys. Rev. B **84**, 024522 (2011).
- ¹⁴ D. K. Singh, S. Kadge, Y. Bang, and P. Majumdar, Fermi Arcs and Pseudogap Phase in a Minimal Microscopic Model of *d*-Wave Superconductivity, Phys. Rev. B **105**, 054501 (2022).
- ¹⁵ A. Kanigel, U. Chatterjee, M. Randeria, M. R. Norman, G. Koren, K. Kadowaki, and J. C. Campuzano, Evidence for Pairing above the Transition Temperature of Cuprate Superconductors from the Electronic Dispersion in the Pseudogap Phase, Phys. Rev. Lett. **101**, 137002 (2008).
- ¹⁶ H. Ding, T. Yokoya, J. C. Campuzano, T. Takahashi, M. Randeria, M. R. Norman, T. Mochiku, K. Kadowaki, and J. Giapintzakis, Spectroscopic Evidence for a Pseudogap in the Normal State of Underdoped High- T_c Superconductors, Nature **382**, 51 (1996).
- ¹⁷ L. Li, Y. Wang, S. Komiya, S. Ono, Y. Ando, G. D. Gu, and N. P. Ong, Diamagnetism and Cooper pairing above T_c in cuprates, Phys. Rev. B **81**, 054510 (2010).
- ¹⁸ K. K. Gomes, A. N. Pasupathy, A. Pushp, S. Ono, Y. Ando, and A. Yazdani, Visualizing Pair Formation on the Atomic Scale in the High- T_c Superconductor $\text{Bi}_2\text{Sr}_2\text{CaCu}_2\text{O}_{8+\delta}$, Nature **447**, 569 (2007).
- ¹⁹ H. B. Yang, J. D. Rameau, P. D. Johnson, T. Valla, A. Tsvelik, and G. D. Gu, Emergence of Preformed Cooper Pairs from the Doped Mott Insulating State in $\text{Bi}_2\text{Sr}_2\text{CaCu}_2\text{O}_{8+\delta}$, Nature **456**, 77 (2008).
- ²⁰ J. Lee, K. Fujita, A. R. Schmidt, C. K. Kim, H. Eisaki, S. Uchida, and J. C. Davis, Spectroscopic Fingerprint of Phase-Incoherent Superconductivity in the Underdoped $\text{Bi}_2\text{Sr}_2\text{CaCu}_2\text{O}_{8+\delta}$, Science **325**, 1099 (2009).
- ²¹ L. S. Bilbro, R. V. Aguilar, G. Logvenov, O. Pelleg, I. Božović, and N. P. Armitage, Temporal Correlations of Superconductivity above the Transition Temperature in $\text{La}_{2-x}\text{Sr}_x\text{CuO}_4$ Probed by Terahertz Spectroscopy, Nat. Phys. **7**, 298 (2011).
- ²² P. Zhou, L. Chen, Y. Liu, I. Sochnikov, A. T. Bollinger, M. G. Han, Y. Zhu, X. He, I. Božović, and D. Natelson, Electron Pairing in the Pseudogap State Revealed by Shot Noise in Copper Oxide Junctions, Nature **572**, 493 (2019).
- ²³ B. Kyung, V. Hankevych, A. M. Daré, and A. M. S. Tremblay, Pseudogap and Spin Fluctuations in the Normal State of the Electron-Doped Cuprates, Phys. Rev. Lett. **93**, 147004 (2004).
- ²⁴ M. Civelli, M. Capone, S. S. Kancharla, O. Parcollet, and G. Kotliar, Dynamical Breakup of the Fermi Surface in a Doped Mott Insulator, Phys. Rev. Lett. **95**, 106402 (2005).
- ²⁵ B. Kyung, S. S. Kancharla, D. Sénéchal, A. M. S. Tremblay, M. Civelli, and G. Kotliar, Pseudogap induced by short-range spin correlations in a doped Mott insulator, Phys. Rev. B **73**, 165114 (2006).
- ²⁶ A. Macridin, M. Jarrell, T. Maier, P. R. C. Kent, and E. D’Azevedo, Pseudogap and Antiferromagnetic Correlations in the Hubbard Model, Phys. Rev. Lett. **97**, 036401 (2006).
- ²⁷ A. Greco, Evidence for Two Competing Order Parameters in Underdoped Cuprate Superconductors from a Model Analysis of Fermi-Arc Effects, Phys. Rev. Lett. **103**, 217001 (2009).
- ²⁸ M. Ferrero, O. Parcollet, A. Georges, G. Kotliar, and D. N. Basov, Interplane charge dynamics in a valence-bond dynamical mean-field theory of cuprate superconductors, Phys. Rev. B **82**, 054502 (2010).
- ²⁹ G. Sordi, P. Sémon, K. Haule, and A. M. S. Tremblay, Pseudogap Temperature as a Widom Line in Doped Mott Insulators, Sci. Rep. **2**, 547 (2012).
- ³⁰ E. Gull, O. Parcollet, and A. J. Millis, Superconductivity and the Pseudogap in the Two-Dimensional Hubbard Model, Phys. Rev. Lett. **110**, 216405 (2013).
- ³¹ W. Wu, M. Ferrero, A. Georges, and E. Kozik, Controlling Feynman diagrammatic expansions: Physical nature of the pseudogap in the two-dimensional Hubbard model, Phys. Rev. B **96**, 041105(R) (2017).
- ³² J. Vučićević, T. Ayril, and O. Parcollet, TRILEX and GW +EDMFT Approach to *d*-wave superconductivity in the Hubbard model, Phys. Rev. B **96**, 104504 (2017).
- ³³ W. Wu, M. S. Scheurer, S. Chatterjee, S. Sachdev, A. Georges, and M. Ferrero, Pseudogap and Fermi-Surface Topology in the Two-Dimensional Hubbard Model, Phys. Rev. X **8**, 021048 (2018).
- ³⁴ A. Richie-Halford, J. E. Drut, and A. Bulgac, Emergence of a Pseudogap in the BCS-BEC Crossover, Phys. Rev. Lett. **125**, 060403 (2020).
- ³⁵ W. Jiang, Y. Liu, A. Klein, Y. Wang, K. Sun, A. V. Chubukov, and Z. Y. Meng, Monte Carlo Study of the Pseudogap and Superconductivity Emerging from Quantum Magnetic Fluctuations, Nat. Commun. **13**, 2655 (2022).
- ³⁶ Z. Long, J. Wang, and Y. Yang, A Slave Fermion Interpretation of the Pseudogap in Doped Mott Insulator, arxiv: 2302.04620 (2023).
- ³⁷ T. Kondo, Y. Hamaya, A. D. Palczewski, T. Takeuchi, J. S. Wen, Z. J. Xu, G. Gu, J. Schmalian, and A. Kaminski, Disentangling Cooper-Pair Formation above the Transition Temperature from the Pseudogap State in the Cuprates, Nat. Phys. **7**, 21 (2011).
- ³⁸ R. H. He, M. Hashimoto, H. Karapetyan, J. D. Koralek, J. P. Hinton, J. P. Testaud, V. Nathan, Y. Yoshida, H. Yao, K. Tanaka, W. Meevasana, R. G. Moore, D. H. Lu, S. K. Mo, M. Ishikado, H. Eisaki, Z. Hussain, T. P. Devereaux, S. A. Kivelson, J. Orenstein, A. Kapitulnik, and Z. X. Shen, From a Single-Band Metal to a High-Temperature Superconductor via Two Thermal Phase Transitions, Science **331**, 1579 (2011).
- ³⁹ A. Kaminski, S. Rosenkranz, H. M. Fretwell, J. C. Campuzano, Z. Li, H. Raffy, W. G. Cullen, H. You, C. G.

- Olson, C. M. Varma, and H. Höchst, Spontaneous Breaking of Time-Reversal Symmetry in the Pseudogap State of a High- T_c Superconductor, *Nature* **416**, 610 (2002).
- ⁴⁰ N. K. Gupta, C. McMahan, R. Sutarto, T. Shi, R. Gong, H. I. Wei, K. M. Shen, F. He, Q. Ma, M. Dragomir, B. D. Gaulin, and D. G. Hawthorn, Vanishing Nematic Order beyond the Pseudogap Phase in Overdoped Cuprate Superconductors, *Proc. Natl. Acad. Sci. U. S. A.* **118**, e2106881118 (2021).
- ⁴¹ P. M. C. Rourke, I. Mouzopoulou, X. Xu, C. Panagopoulos, Y. Wang, B. Vignolle, C. Proust, E. V. Kurganova, U. Zeitler, Y. Tanabe, T. Adachi, Y. Koike, and N. E. Hussey, Phase-Fluctuating Superconductivity in Overdoped $\text{La}_{2-x}\text{Sr}_x\text{CuO}_4$, *Nat. Phys.* **7**, 455 (2011).
- ⁴² I. Bozovic, X. He, J. Wu, and A. T. Bollinger, Dependence of the Critical Temperature in Overdoped Copper Oxides on Superfluid Density, *Nature* **536**, 309 (2016).
- ⁴³ F. Mahmood, X. He, I. Božović, and N. P. Armitage, Locating the Missing Superconducting Electrons in the Overdoped Cuprates $\text{La}_{2-x}\text{Sr}_x\text{CuO}_4$, *Phys. Rev. Lett.* **122**, 027003 (2019).
- ⁴⁴ Y. He, S. Di Chen, Z. X. Li, D. Zhao, D. Song, Y. Yoshida, H. Eisaki, T. Wu, X. H. Chen, D. H. Lu, C. Meingast, T. P. Devereaux, R. J. Birgeneau, M. Hashimoto, D. H. Lee, and Z. X. Shen, Superconducting Fluctuations in Overdoped $\text{Bi}_2\text{Sr}_2\text{CaCu}_2\text{O}_{8+\delta}$, *Phys. Rev. X* **11**, 031068 (2021).
- ⁴⁵ S. Di Chen, M. Hashimoto, Y. He, D. Song, J. F. He, Y. F. Li, S. Ishida, H. Eisaki, J. Zaanen, T. P. Devereaux, D. H. Lee, D. H. Lu, and Z. X. Shen, Unconventional Spectral Signature of T_c in a Pure d -Wave Superconductor, *Nature* **601**, 562 (2022).
- ⁴⁶ C. Zou, Z. Hao, X. Luo, S. Ye, Q. Gao, M. Xu, X. Li, P. Cai, C. Lin, X. Zhou, D.-H. Lee, and Y. Wang, Particle-Hole Asymmetric Superconducting Coherence Peaks in Overdoped Cuprates, *Nat. Phys.* **18**, 551 (2022).
- ⁴⁷ D. Wang, J. Xu, H. Zhang, and Q. Wang, Anisotropic Scattering Caused by Apical Oxygen Vacancies in Thin Films of Overdoped High-Temperature Cuprate Superconductors, *Phys. Rev. Lett.* **128**, 137001 (2022).
- ⁴⁸ N. R. Lee-Hone, V. Mishra, D. M. Broun, and P. J. Hirschfeld, Optical Conductivity of Overdoped Cuprate Superconductors: Application to $\text{La}_{2-x}\text{Sr}_x\text{CuO}_4$, *Phys. Rev. B* **98**, 054506 (2018).
- ⁴⁹ Z. X. Li, S. A. Kivelson, and D. H. Lee, Superconductor-to-Metal Transition in Overdoped Cuprates, *npj Quantum Mater.* **6**, 36 (2021).
- ⁵⁰ W. Wéi, W. Xiang, and T. André-Marie, Non-Fermi Liquid Phase and Linear-in-Temperature Scattering Rate in Overdoped Two-Dimensional Hubbard Model, *Proc. Natl. Acad. Sci. (U.S.A.)* **119**, e2115819119 (2022).
- ⁵¹ J.-J. Dong, D. Huang, and Y. Yang, Mutual information, quantum phase transition and phase coherence in Kondo systems, *Phys. Rev. B* **104**, L081115 (2021).
- ⁵² A. Mukherjee, N. D. Patel, S. Dong, S. Johnston, A. Moreo, and E. Dagotto, Testing the Monte Carlo-Mean field approximation in the one-band Hubbard model, *Phys. Rev. B* **90**, 205133 (2014).
- ⁵³ S. Liang, A. Moreo, and E. Dagotto, Nematic State of Pnictides Stabilized by Interplay between Spin, Orbital, and Lattice Degrees of Freedom, *Phys. Rev. Lett.* **111**, 047004 (2013).
- ⁵⁴ Y. Dubi, Y. Meir, and Y. Avishai, Nature of the Superconductor-Insulator Transition in Disordered Superconductors, *Nature* **449**, 876 (2007).
- ⁵⁵ K. Pasrija, P. B. Chakraborty, and S. Kumar, Effective Hamiltonian based Monte Carlo for the BCS to BEC crossover in the attractive Hubbard model, *Phys. Rev. B* **94**, 165150 (2016).
- ⁵⁶ M. Karmakar, Pauli Limited d -Wave Superconductors: Quantum Breached Pair Phase and Thermal Transitions, *J. Phys. Condens. Matter* **32**, 405604 (2020).
- ⁵⁷ T. M. Cover and J. A. Thomas, *Elements of Information Theory* (Wiley Series in Telecommunications and Signal Processing) (Wiley-Interscience, USA, 2006).
- ⁵⁸ A. Kraskov, H. Stögbauer, and P. Grassberger, Estimating mutual information, *Phys. Rev. E* **69**, 066138 (2004).
- ⁵⁹ M. K. Varanasi, Estimation of the Information by an Adaptive Partitioning of the Observation Space Georges, *IEEE Trans. Inf. Theory* **45**, 1315 (1999).
- ⁶⁰ S. Gao, G. Ver Steeg, and A. Galstyan, Efficient Estimation of Mutual Information for Strongly Dependent Variables, in *Proceedings of the 18th International Conference on Artificial Intelligence and Statistics* (PMLR, 2015), Vol. 38, p. 277.
- ⁶¹ S. Khan, S. Bandyopadhyay, A. R. Ganguly, S. Saigal, D. J. Erickson, V. Protopopescu, and G. Ostrouchov, Relative performance of mutual information estimation methods for quantifying the dependence among short and noisy data, *Phys. Rev. E* **76**, 026209 (2007).
- ⁶² M. I. Belghazi, A. Baratin, S. Rajeswar, S. Ozair, Y. Bengio, A. Courville, and R. D. Hjelm, Mutual Information Neural Estimation, in *Proceedings of the 35th International Conference on Machine Learning* (PMLR, 2018), Vol. 80, pp. 531-540.
- ⁶³ B. Poole, S. Ozair, A. V. D. Oord, A. A. Alemi, and G. Tucker, On Variational Bounds of Mutual Information, in *Proceedings of the 36th International Conference on Machine Learning, Long Beach, California* (PMLR, 2019), Vol. 97, p. 5171.
- ⁶⁴ T. Speed, A Correlation for the 21st Century (*Science* (2011) (1502)), *Science* **334**, 1502 (2012).
- ⁶⁵ D. Reshef, Y. Reshef, H. Finucane, S. Grossman, G. Mcvean, P. Turnbaugh, E. Lander, M. Mitzenmacher, and P. Sabeti, Detecting Novel Associations in Large Data Sets, *Science* **334**, 1518 (2011).
- ⁶⁶ J. B. Kinney and G. S. Atwal, Equitability, Mutual Information, and the Maximal Information Coefficient, *Proc. Natl. Acad. Sci. (U.S.A.)* **111**, 3354 (2014).
- ⁶⁷ M. Koch-Janusz and Z. Ringel, Mutual Information, Neural Networks and the Renormalization Group, *Nat. Phys.* **14**, 578 (2018).
- ⁶⁸ A. Nir, E. Sela, R. Beck, and Y. Bar-Sinai, Machine-Learning Iterative Calculation of Entropy for Physical Systems, *Proc. Natl. Acad. Sci. (U.S.A.)* **117**, 30234 (2020).
- ⁶⁹ D. E. Gökmen, Z. Ringel, S. D. Huber, and M. Koch-Janusz, Statistical Physics through the Lens of Real-Space Mutual Information, *Phys. Rev. Lett.* **127**, 240603 (2021).
- ⁷⁰ F. Parisen Toldin, T. Sato, and F. F. Assaad, Mutual information in heavy-fermion systems, *Phys. Rev. B* **99**, 155158 (2019).
- ⁷¹ C. Walsh, M. Charlebois, P. Sémon, G. Sordi, and A. M. S. Tremblay, Information-Theoretic Measures of Superconductivity in a Two-Dimensional Doped Mott Insulator, *Proc. Natl. Acad. Sci. (U.S.A.)* **118**, e2104114118 (2021).
- ⁷² G. Nicoletti and D. M. Busiello, Mutual Information

- Disentangles Interactions from Changing Environments, Phys. Rev. Lett. **127**, 228301 (2021).
- ⁷³ H. Kim, Y. Choi, C. Lewandowski, A. Thomson, Y. Zhang, R. Polski, K. Watanabe, T. Taniguchi, J. Alicea, and S. Nadj-Perge, Evidence for Unconventional Superconductivity in Twisted Trilayer Graphene, Nature **606**, 494 (2022).
- ⁷⁴ P. Monthoux, D. Pines, and G. G. Lonzarich, Superconductivity without Phonons, Nature **450**, 1177 (2007).
- ⁷⁵ P. Coleman, *Introduction to Many-body Physics*, (Cambridge University Press, Cambridge, England, 2015).
- ⁷⁶ J. P. Carbotte, Properties of a two-dimensional d -wave superconductor from phenomenological susceptibility, Phys. Rev. B **49**, 4176 (1994).
- ⁷⁷ P. Monthoux and G. G. Lonzarich, Magnetically mediated superconductivity in quasi-two and three Dimensions, Phys. Rev. B **63**, 054529 (2001).
- ⁷⁸ M. Platié, J. D. F. Mottershead, I. S. Elfimov, D. C. Peets, R. Liang, D. A. Bonn, W. N. Hardy, S. Chizbaian, M. Falub, M. Shi, L. Patthey, and A. Damascelli, Fermi Surface and Quasiparticle Excitations of Overdoped $Tl_2Ba_2CuO_{6+\delta}$, Phys. Rev. Lett. **95**, 077001 (2005).
- ⁷⁹ B. Vignolle, A. Carrington, R. A. Cooper, M. M. J. French, A. P. Mackenzie, C. Jaudet, D. Vignolles, C. Proust, and N. E. Hussey, Quantum Oscillations in an Overdoped High- T_c Superconductor, Nature **455**, 952 (2008).
- ⁸⁰ P. Monthoux, A. V Balatsky, and D. Pines, Toward a Theory of High-Temperature Superconductivity in the Antiferromagnetically Correlated Cuprate Oxides, Phys. Rev. Lett. **67**, 3448 (1991).
- ⁸¹ V. L. Berezinskii, Destruction of Long-Range Order in One-Dimensional and Two-Dimensional Systems Possessing a Continuous Symmetry Group. II. Quantum Systems, Zh. Eksp. Teor. Fiz. **61**, 1144 (1971) [Sov. Phys. JETP **34**, 610 (1972)].
- ⁸² J. M. Kosterlitz and D. J. Thouless, Ordering, Metastability and Phase Transitions in Two-Dimensional Systems, J. Phys. C **6**, 1181 (1973).
- ⁸³ J. M. Kosterlitz, The Critical Properties of the Two-Dimensional XY Model, J. Phys. C **7**, 1046 (1974).
- ⁸⁴ J. Li, C. Cheng, T. Paiva, H.-Q. Lin, and R. Mondaini, Giant Magnetoresistance in Hubbard Chains, Phys. Rev. Lett. **121**, 020403 (2018).
- ⁸⁵ N. Harrison, R. D. McDonald, and J. Singleton, Cuprate Fermi Orbits and Fermi Arcs: The Effect of Short-Range Antiferromagnetic Order, Phys. Rev. Lett. **99**, 206406 (2007).
- ⁸⁶ G. Alvarez and E. Dagotto, Fermi Arcs in the Superconducting Clustered State for Underdoped Cuprate Superconductors, Phys. Rev. Lett. **101**, 177001 (2008).
- ⁸⁷ A. Kanigel, M. R. Norman, M. Randeria, U. Chatterjee, S. Souma, A. Kaminski, H. M. Fretwell, S. Rosenkranz, M. Shi, T. Sato, T. Takahashi, Z. Z. Li, H. Raffy, K. Kadowaki, D. Hinks, L. Ozyuzer, and J. C. Campuzano, Evolution of the Pseudogap from Fermi Arcs to the Nodal Liquid, Nat. Phys. **2**, 447 (2006).
- ⁸⁸ T. J. Reber, N. C. Plumb, Z. Sun, Y. Cao, Q. Wang, K. McElroy, H. Iwasawa, M. Arita, J. S. Wen, Z. J. Xu, G. Gu, Y. Yoshida, H. Eisaki, Y. Aiura, and D. S. Dessau, The Origin and Non-Quasiparticle Nature of Fermi Arcs in $Bi_2Sr_2CaCu_2O_{8+\delta}$, Nat. Phys. **8**, 606 (2012).
- ⁸⁹ M. Danilov, E. G. C. P. van Loon, S. Brener, S. Isakov, M. I. Katsnelson, and A. I. Lichtenstein, Degenerate plaquette physics as key ingredient of high-temperature superconductivity in cuprates, Npj Quantum Mater. **7**, 50 (2022).
- ⁹⁰ A. Nazarenko, A. Moreo, E. Dagotto, and J. Riera, Superconductivity in a model of correlated fermions, Phys. Rev. B **54**, R768 (1996).
- ⁹¹ M. Shaw and W. P. Su, Phase Separation Due to Nearest Neighbor Attractive Interactions in a Two-Dimensional Model, Mod. Phys. Lett. B **17**, 853 (2003).
- ⁹² W. P. Su, Phase separation and d -wave superconductivity in a two-dimensional extended Hubbard model with nearest-neighbor attractive interaction, Phys. Rev. B **69**, 012506 (2004).
- ⁹³ V. J. Emery, Phase Separation in the t - J model, Phys. Rev. Lett. **64**, 475 (1990).
- ⁹⁴ M. D. Cookson and P. M. R. Stirk, Indications of $d_{x^2-y^2}$ Superconductivity in the Two Dimensional t - J Model, Phys. Rev. Lett. **70**, 682 (1993).
- ⁹⁵ P. A. Lee, Amperean Pairing and the Pseudogap Phase of Cuprate Superconductors, Phys. Rev. X **4**, 031017 (2014).
- ⁹⁶ C. Setty, L. Fanfarillo, and P. J. Hirschfeld, Mechanism for Fluctuating Pair Density Wave, Nat. Commun. **14**, 3181 (2023).
- ⁹⁷ C. Setty, J. Zhao, L. Fanfarillo, E. W. Huang, P. J. Hirschfeld, P. W. Phillips, and K. Yang, Exact Solution for Finite Center-of-Mass Momentum Cooper Pairing, arXiv:2209.10568 (2022).
- ⁹⁸ Z. Chen, Y. Wang, S. N. Rebec, T. Jia, M. Hashimoto, D. Lu, B. Moritz, R. G. Moore, T. P. Devereaux, and Z. X. Shen, Anomalously Strong Near-Neighbor Attraction in Doped 1D Cuprate Chains, Science **373**, 1235 (2021).
- ⁹⁹ N. Plonka, C. J. Jia, Y. Wang, B. Moritz, and T. P. Devereaux, Fidelity study of superconductivity in extended Hubbard models, Phys. Rev. B **92**, 024503 (2015).
- ¹⁰⁰ M. Jiang, Enhancing d -wave superconductivity with nearest-neighbor attraction in the extended Hubbard model, Phys. Rev. B **105**, 024510 (2022).
- ¹⁰¹ S. M. O'Mahony, W. Ren, W. Chen, Y. X. Chong, X. Liu, H. Eisaki, S. Uchida, M. H. Hamidian, and J. C. S. Davis, On the Electron Pairing Mechanism of Copper-Oxide High Temperature Superconductivity, Proc. Natl. Acad. Sci. (U. S. A.) **119**, e2207449119 (2022).
- ¹⁰² L. Wang, G. He, Z. Yang, M. Garcia-Fernandez, A. Nag, K. Zhou, M. Minola, M. Le Tacon, B. Keimer, Y. Peng, and Y. Li, Paramagnons and High-Temperature Superconductivity in a Model Family of Cuprates, Nat. Commun. **13**, 3163 (2022).
- ¹⁰³ A. Paramekanti, M. Randeria, T. V. Ramakrishnan, and S. S. Mandal, Effective actions and phase fluctuations in d -wave superconductors, Phys. Rev. B **62**, 6786 (2000).
- ¹⁰⁴ N. D. Mermin, Crystalline Order in Two Dimensions, Phys. Rev. **176**, 250 (1968).
- ¹⁰⁵ P. C. Hohenberg, Existence of Long-Range Order in One and Two Dimensions, Phys. Rev. **158**, 383 (1967).
- ¹⁰⁶ B. Spivak, P. Oretto, and S. A. Kivelson, Theory of quantum metal to superconductor transitions in highly conducting systems, Phys. Rev. B **77**, 214523 (2008).
- ¹⁰⁷ A. Kapitulnik, S. A. Kivelson, and B. Spivak, Colloquium: Anomalous Metals: Failed Superconductors, Rev. Mod. Phys. **91**, 11002 (2019).
- ¹⁰⁸ Y. Xu, H. Rong, Q. Wang, D. Wu, Y. Hu, Y. Cai, Q. Gao, H. Yan, C. Li, C. Yin, H. Chen, J. Huang, Z. Zhu, Y. Huang, G. Liu, Z. Xu, L. Zhao, and X. J. Zhou, Spec-

- troscopic Evidence of Superconductivity Pairing at 83 K in Single-Layer FeSe/SrTiO₃ Films, *Nat. Commun.* **12**, 2840 (2021).
- ¹⁰⁹ B. D. Faeth, S. L. Yang, J. K. Kawasaki, J. N. Nelson, P. Mishra, C. T. Parzyck, C. Li, D. G. Schlom, and K. M. Shen, Incoherent Cooper Pairing and Pseudogap Behavior in Single-Layer FeSe/SrTiO₃, *Phys. Rev. X* **11**, 021054 (2021).
- ¹¹⁰ B. L. Kang, M. Z. Shi, S. J. Li, H. H. Wang, Q. Zhang, D. Zhao, J. Li, D. W. Song, L. X. Zheng, L. P. Nie, T. Wu, and X. H. Chen, Preformed Cooper Pairs in Layered FeSe-Based Superconductors, *Phys. Rev. Lett.* **125**, 097003 (2020).
- ¹¹¹ V. Grinenko, D. Weston, F. Caglieris, C. Wuttke, C. Hess, T. Gottschall, I. Maccari, D. Gorbunov, S. Zherlitsyn, J. Wosnitzer, A. Rydh, K. Kihou, C.-H. Lee, R. Sarkar, S. Dengre, J. Garaud, A. Charnukha, R. Hühne, K. Nielsch, B. Büchner, H.-H. Klauss, and E. Babaev, State with Spontaneously Broken Time-Reversal Symmetry above the Superconducting Phase Transition, *Nat. Phys.* **17**, 1254 (2021).
- ¹¹² T. Dubouchet, B. Sacépé, J. Seidemann, D. Shahar, M. Sanquer, and C. Chapelier, Collective Energy Gap of Preformed Cooper Pairs in Disordered Superconductors, *Nat. Phys.* **15**, 233 (2019).
- ¹¹³ K. M. Bastiaans, D. Chatzopoulos, J.-F. Ge, D. Cho, W. O. Tromp, J. M. van Ruitenbeek, M. H. Fischer, P. J. de Visser, D. J. Thoen, E. F. C. Driessen, T. M. Klapwijk, and M. P. Allan, Direct Evidence for Cooper Pairing without a Spectral Gap in a Disordered Superconductor above T_C , *Science* **374**, 608 (2021).
- ¹¹⁴ M. Mondal, A. Kamlapure, M. Chand, G. Saraswat, S. Kumar, J. Jesudasan, L. Benfatto, V. Tripathi, and P. Raychaudhuri, Phase Fluctuations in a Strongly Disordered S-Wave Nbn Superconductor Close to the Metal-Insulator Transition, *Phys. Rev. Lett.* **106**, 047001 (2011).
- ¹¹⁵ Z. Chen, A. G. Swartz, H. Yoon, H. Inoue, T. A. Merz, D. Lu, Y. Xie, H. Yuan, Y. Hikita, S. Raghu, and H. Y. Hwang, Carrier Density and Disorder Tuned Superconductor-Metal Transition in a Two-Dimensional Electron System, *Nat. Commun.* **9**, 4008 (2018).
- ¹¹⁶ K. Bouadim, Y. L. Loh, M. Randeria, and N. Trivedi, Single- and Two-Particle Energy Gaps across the Disorder-Driven Superconductor-Insulator Transition, *Nat. Phys.* **7**, 884 (2011).
- ¹¹⁷ A. Ghosal, M. Randeria, and N. Trivedi, Role of Spatial Amplitude Fluctuations in Highly Disordered *s*-Wave Superconductors, *Phys. Rev. Lett.* **81**, 3940 (1998).
- ¹¹⁸ Q. Cui and K. Yang, Fulde-Ferrell-Larkin-Ovchinnikov state in disordered *s*-wave superconductors, *Phys. Rev. B* **78**, 054501 (2008).